aerospace

MDPI

Article

Design of Convergent and Accurate Guidance Law with Finite Time in Complex Adversarial Scenarios

Hang Ding [1], Dongdong Wang [2], Chuanjun Li [1,*], Xiao Liang [1,*] and Xingcheng Li [1]

[1] School of Aerospace Engineering, Beijing Institute of Technology, Beijing 100081, China; bitdinghang@163.com (H.D.); xingchli@bit.edu.cn (X.L.)
[2] Beijing Institute of Space Long March Vehicle, Beijing 100081, China; ddwang1992@163.com
* Correspondence: lichuanjun@bit.edu.cn (C.L.); liang.xiao@bit.edu.cn (X.L.)

Abstract: The target can deceive the flight vehicle by releasing an infrared decoy to make the line-of-sight (LOS) angle rate deflect greatly, thus causing the flight vehicle to miss the target. Therefore, in order to accurately strike the target in complex adversarial scenarios, this paper proposes a finite-time convergence guidance law (FTCG) combined with a finite-time disturbance observer (FTDO). The complex adversarial scenario is established by combining the relative motion model between the flight vehicle and the target and the motion model of the infrared decoy. Based on this, considering the dynamic characteristic of the flight vehicle's autopilot, a guidance model is obtained. Utilizing sliding mode control theory and finite-time control theory, an FTCG of the LOS angle rate is designed. Then, the finite-time convergence of the guidance law is proved and the total convergence time is derived. Finally, for the target maneuvering that is difficult to measure in the guidance law, an FTDO is used to estimate and compensate for the target maneuvering in the guidance law. Simulation results show that the FTCG can make the LOS angle rate quickly converge and accurately strike the target in different scenarios, with a good guidance accuracy and robustness. Compared with the sliding mode guidance law (SMGL) and the adaptive sliding mode guidance law (ASMGL) based on an extended state observer (ESO), the advantages of the designed guidance law are illustrated. Finally, FTCG is extended to be three dimensional and compared with the proportional navigation guidance law (PNG) to further illustrate its effectiveness in a three-dimensional coordinate system.

Keywords: complex adversarial scenarios; finite-time convergence guidance law; finite-time disturbance observer; infrared decoy

Citation: Ding, H.; Wang, D.; Li, C.; Liang, X.; Li, X. Design of Convergent and Accurate Guidance Law with Finite Time in Complex Adversarial Scenarios. *Aerospace* **2024**, *11*, 56. https://doi.org/10.3390/aerospace11010056

Academic Editor: Gokhan Inalhan

Received: 13 November 2023
Revised: 4 January 2024
Accepted: 5 January 2024
Published: 7 January 2024

1. Introduction

With continuous changes in the form of warfare, the operational environment faced by infrared precision weapon systems is becoming increasingly harsh, which greatly reduces the probability and the accuracy of flight vehicle hits. Therefore, higher requirements are put forward for the precise strike capability of terminal guidance [1]. In complex adversarial scenarios, a target aircraft not only performs maneuvers but also uses the deployment of an infrared decoy to deceive the infrared imaging seeker, causing the seeker to identify the equivalent radiation energy center between the target and the infrared decoy. When the seeker's head re-identifies the target, it will cause a sudden change in the LOS angle rate, then a sudden change in flight vehicle guidance commands. The divergence of the LOS angle rate at the final guidance time will lead to a sharp increase in the required overload, which may lead to the loss of stability of the guidance loop and affect the accurate guidance of the flight vehicle. Therefore, it is necessary to study the improvement of robustness of the accurate guidance law.

Currently, there have been many studies on the influence of infrared decoys on flight vehicle guidance accuracy. Reference [1] established a complex adversarial scenario composed of a guidance model and an infrared decoy motion model and analyzed the effects of the deployment distance of infrared decoys, the recognition time of the seeker, and the deployment interval of multiple infrared decoys on the guidance accuracy. The adjoint method is used to analyze the effects of the target barrel roll rate, the number of simultaneous deployments of point source decoys, and the deployment interval on the miss distance in Reference [2]. Reference [3] analyzed the miss distance and anti-jamming probability of different anti-jamming methods for seekers in complex adversarial scenarios. The guidance laws mentioned in the above references are all analyzed using the PNG, indicating that infrared decoys have a significant impact on the PNG. Both the PNG and SMGL are used by the miss distance in complex adversarial scenarios, and the SMGL has better robustness than the PNG in Reference [4].

The above references are based on traditional guidance laws for attack and propose anti-interference algorithms based on the algorithm of the seeker head, without using more robust and accurate modern guidance laws for simulation verification. Currently, various modern control methods are applied in the field of flight vehicle guidance, such as sliding mode control [5–7], finite-time control [8–10], optimal control [11–13], etc. However, many modern guidance laws are designed based on asymptotic stability. Only when time tends to infinity will the LOS angle rate converge. Therefore, using finite-time control theory to derive guidance laws can make the LOS angle rate converge within a finite time. References [14–16] respectively use finite-time control theory to derive guidance laws with finite-time convergence of the LOS angle rate and prove their finite-time convergence. However, the above references consider the target maneuver as a bounded disturbance compensation in the guidance law, without accurate estimation of the target maneuver. In References [10,17–20], an ESO is used to observe and compensate for the target maneuver in real time, solve the problem of excessive overload in the terminal guidance process effectively, and provide the flight vehicle with a higher interception accuracy. References [7,21,22] adopt an FTDO to estimate the target maneuver. The guidance laws and observers in the above references can accurately hit targets and accurately estimate target maneuvers under normal adversarial scenarios. However, these methods have not been applied in complex adversarial scenarios, so their undetermined robustness and accuracy limits the application in reality.

In response to the limited application of advanced guidance laws in complex adversarial scenarios, this paper proposes an FTCG that takes into account the dynamic characteristic of the autopilot based on sliding mode control theory and finite-time control theory. The FTCG combines with an FTDO to be applied in complex adversarial scenarios, aiming to determine its accuracy and robustness and provide an idea for confronting infrared decoys.

The remaining structure of this article is as follows: problem statement and preliminaries, design and analysis of guidance law, simulation results and analysis, and discussion. In Section 2, a complex adversarial scenario composed of the flight vehicle, the target, and the infrared decoy is constructed, and the foundation of finite-time control theory is elucidated. In Section 3, an FTCG considering the dynamic characteristics of the autopilot is derived through finite-time control theory. Its stability and convergence are proved, and an FTDO is used to estimate and compensate for the target maneuvering into the guidance law. In Section 4, the guidance law is validated and analyzed in different complex adversarial scenarios and compared with other guidance laws to mainly analyze its accuracy and robustness. Finally, the conclusions of this study are summarized in Section 5.

2. Problem Statement and Preliminaries

2.1. Problem Statement

Figure 1 represents the relative motion relationship between the flight vehicle and the target in the two-dimensional longitudinal plane. In the figure, M represents the position of the flight vehicle's center of mass; T represents the position of the target's center of mass; V_M and V_T respectively represent the velocity values of the flight vehicle and the target. In order to simplify the mathematical model, the derivatives of the velocity of the flight vehicle and the target are assumed to be $\dot{V}_M = 0$ and $\dot{V}_T = 0$; A_M and A_T respectively represent the normal acceleration of the flight vehicle and the target; θ_M and θ_T respectively represent the trajectory inclination of the flight vehicle and the target; q represents LOS angle; r represents the relative range from the flight vehicle to the target.

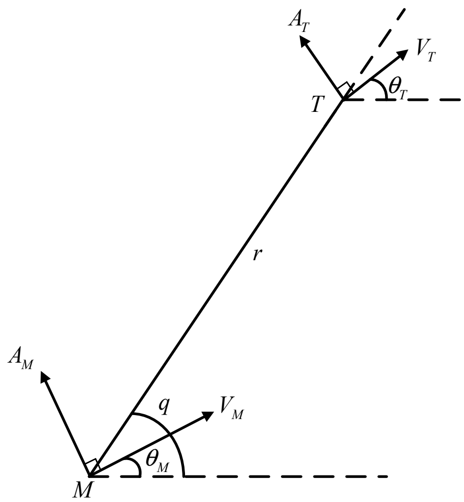

Figure 1. Relative motion relationship.

From Figure 1, the equation of the relative motion relationship can be obtained as follows:

$$\begin{cases} \dot{r} = V_T \cos(q - \theta_T) - V_M \cos(q - \theta_M) \\ r\dot{q} = -V_T \sin(q - \theta_T) + V_M \sin(q - \theta_M) \end{cases} \tag{1}$$

According to the relationship between normal acceleration and trajectory inclination, the following can be obtained:

$$\begin{cases} A_M = \dot{\theta}_M V_M \\ A_T = \dot{\theta}_T V_T \end{cases} \tag{2}$$

where $\dot{\theta}_M$ and $\dot{\theta}_T$ respectively represent the derivative of trajectory inclination of the flight vehicle and the target.

Differentiating both sides of the second equation in Equation (1), the following can be obtained:

$$\ddot{q} = \frac{-2\dot{r}}{r}\dot{q} - \frac{A_M \cos(q - \theta_M)}{r} + \frac{A_T \cos(q - \theta_T)}{r} \tag{3}$$

In order to facilitate the calculation, the variables in Equation (3) are redefined, so that $A_{Mq} = A_M \cos(q - \theta_M)$ and $A_{Tq} = A_T \cos(q - \theta_T)$. Equation (3) can be expressed as follows:

$$\ddot{q} = \frac{-2\dot{r}}{r}\dot{q} - \frac{A_{Mq}}{r} + \frac{A_{Tq}}{r} \tag{4}$$

A_{Mq} and A_{Tq} in Equation (4) are, respectively, the components of the acceleration of the flight vehicle and the target perpendicular to the LOS.

An infrared decoy is generally divided into a point-source decoy projectile and surface-source decoy projectile, according to the radiation characteristics. This paper analyzes the point-source decoy projectile. After being launched, the infrared point-source decoy projectiles will generate infrared radiation in a specific spectral range, thus deceiving the detection system. During the target recognition process by the guidance head, both the interference and target will appear in the field of view of the guidance head, and the guidance head tracks the equivalent energy center of the two. When the image-processing algorithm re-identifies the target, the guidance head will jump back from the equivalent energy center to the target, and the jumping of the tracking instructions has an adverse effect on the guidance [1]. Figure 2 shows the specific process, where H represents the infrared decoy.

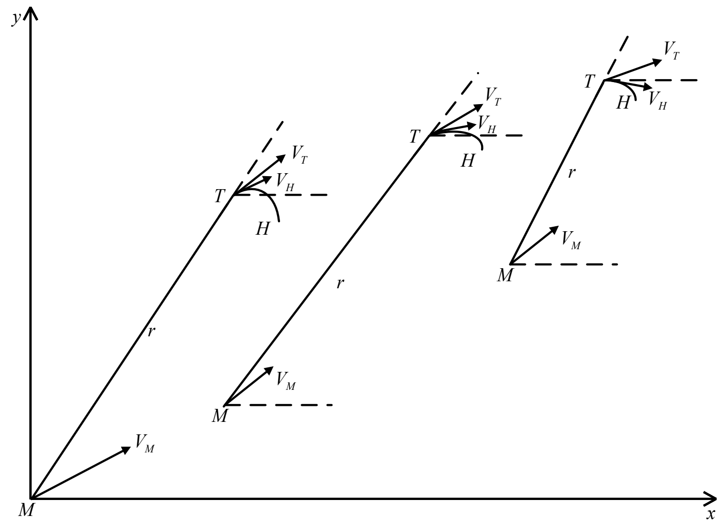

Figure 2. Schematic diagram of the infrared decoy interference process.

The infrared decoy is mainly affected by gravity and the aerodynamic force after launch, and its motion equation in the two-dimensional longitudinal plane is as follows:

$$\begin{cases} m_H \frac{dV_{Hx}}{dt} = -f \frac{V_{Hx}}{V_H} \\ m_H \frac{dV_{Hy}}{dt} = -f \frac{V_{Hy}}{V_H} - m_H g \\ f = \frac{1}{2} C_H S \rho V_H^2 \\ m_H = m_{H0} - \dot{m}_H t \end{cases} \tag{5}$$

In the formula, m_H is the mass of the infrared decoy, m_{H0} is the initial mass of the infrared decoy, and $\dot{m}_H$ is the mass consumption rate of the infrared decoy; f is the resistance of the infrared decoy, C_H is the resistance coefficient of the infrared decoy, S is the area of the infrared decoy, and ρ is the atmospheric density; V_H is the velocity of the infrared decoy, V_{Hx} and V_{Hy} are the components of the infrared decoy velocity in the coordinate system.

According to the principle of centroid interference [2], when the seeker cannot distinguish the real target from the infrared decoy for a period of time, the LOS is usually directed to the energy center of the two. The motion equation of the energy center in the Y direction is as follows:

$$\begin{cases} y_N = y_H K_H + y_T (1 - K_H) \\ V_{Ny} = V_{Hy} K_H + V_{Ty} (1 - K_H) \\ A_{Ny} = A_{Hy} K_H + A_{Ty} (1 - K_H) \\ K_H = nK/(nK + 1) \\ K = W_H / W_T \end{cases} \tag{6}$$

In the formula, y_N, V_{Ny}, and A_{Ny} are, respectively, the position, velocity and acceleration in the Y direction of the energy center; y_H, V_{Hy}, and A_{Hy} are, respectively, the position, velocity, and acceleration in the Y direction of the infrared decoy; y_T, V_{Ty}, and A_{Ty} are, respectively, the position, velocity, and acceleration in the Y direction of the target; K is the suppression coefficient, generally between 2 and 3; W_H and W_T respectively represent the radiation intensity of a single infrared decoy and the radiation intensity of the target, n is the number of infrared decoy launched at one time. The motion equation of the energy center in the X direction is similar to that in the Y direction.

2.2. Preliminaries

Definition 1 ([23]). *Consider the following nonlinear system:*

$$\dot{x} = f(x,t), f(0,t) = 0, x \in R^n \tag{7}$$

where $f : U_0 \times R \to R^n$ is continuous over $U_0 \times R$, and U_0 is an open field of the origin $x = 0$. The equilibrium point of the system $x = 0$ converges in finite time, which means that for the initial state $x(t_0) = x_0 \in U$ given at any initial time t_0, there is a resting time $T \geq 0$ that depends on x_0, so that the solution $x(t) = \varphi(t; t, x_0)$ of Equation (7) with x_0 as the initial state is defined, and:

$$\begin{cases} \lim\limits_{t \to T(x_0)} \varphi(t; t_0, x_0) = 0 \\ \varphi(t; t_0, x_0) = 0,\ t > T(x_0) \end{cases} \tag{8}$$

when $t \in [t_0, T(x_0)]$, $\varphi(t; t_0, x_0) \in U/\{0\}$.

Based on finite-time control theory, there is Lemma 1 as follows:

Lemma 1 ([23]). *Consider the nonlinear system (7), assuming the existence of a smooth function defined in the domain $\widehat{U} \subset R^n$ at the origin, and the existence of real values $\alpha > 0$ and $0 < \lambda < 1$ such that $V(x)$ is a positive definite on $\widehat{U}$ and $\dot{V}(x) + \alpha V^\lambda(x)$ a semi-negative definite on $\widehat{U}$, then the origin of the system is finite-time stable. Its stability time t_e is related to the initial value $x(0) = x_0$, there is $V(x)|_{t=0} = V(x_0)$, and the upper bound of its stability time is as follows:*

$$t_e \leq \frac{V^{1-\lambda}(x_0)}{\alpha(1-\lambda)} \tag{9}$$

3. Design and Analysis of Guidance Law

3.1. Design of FTCG

Equation (4) is the relative motion equation but this equation does not take into account the dynamic characteristics of autopilot. Considering the dynamic characteristic is first-order, it can be obtained as follows:

$$\dot{A}_{Mq} = -\frac{1}{\tau} A_{Mq} + \frac{1}{\tau} A_{Mc} \tag{10}$$

where τ is the time constant of autopilot, A_{Mc} is the guidance command and guidance law provided to the autopilot, and A_{Mq} is the actual overload of the flight vehicle.

Defining $x_1 = \dot{q}$ and $x_2 = \ddot{q}$, Equation (4) can be rewritten as follows:

$$x_2 = \frac{-2\dot{r}}{r} x_1 - \frac{A_{Mq}}{r} + \frac{A_{Tq}}{r} \tag{11}$$

According to Equation (11), the following can be obtained:

$$A_{Tq} = A_{Mq} + r x_2 + 2\dot{r} x_1 \tag{12}$$

By differentiating x_2, the following can be obtained:

$$\dot{x}_2 = -\frac{2\ddot{r}r - 2\dot{r}^2}{r^2} x_1 - \frac{2\dot{r}}{r} x_2 + \frac{1}{r^2} A_{Mq} - \frac{1}{r} \dot{A}_{Mq} - \frac{1}{r^2} A_{Tq} + \frac{1}{r} \dot{A}_{Tq} \tag{13}$$

By substituting Equations (10) and (12) into Equation (13), the following can be obtained:

$$\dot{x}_2 = \frac{2\dot{r}^2 - 2\ddot{r}r - 2\dot{r}}{r^2} x_1 - \frac{2\dot{r} + 1}{r} x_2 + \frac{1}{r\tau} A_{Mq} - \frac{1}{r\tau} A_{Mc} + \frac{1}{r} \dot{A}_{Tq} \tag{14}$$

In the terminal guidance process, the change in $\dot{r}$ is small and usually $\ddot{r} = 0$ can be assumed, then Equation (14) can be simplified as follows:

$$\dot{x}_2 = \frac{2\dot{r}^2 - 2\dot{r}}{r^2}x_1 - \frac{2\dot{r}+1}{r}x_2 + \frac{1}{r\tau}A_{Mq} - \frac{1}{r\tau}A_{Mc} + \frac{1}{r}\dot{A}_{Tq} \tag{15}$$

The guidance equation composed of Equations (11) and (15) considering the first-order dynamic characteristics of the autopilot is as follows:

$$\begin{bmatrix} \dot{x}_1 \\ \dot{x}_2 \end{bmatrix} = \begin{bmatrix} 0 & 1 \\ A_1 & A_2 \end{bmatrix}\begin{bmatrix} x_1 \\ x_2 \end{bmatrix} + \begin{bmatrix} 0 \\ B \end{bmatrix}A_{Mq} - \begin{bmatrix} 0 \\ B \end{bmatrix}A_{Mc} + \begin{bmatrix} 0 \\ C \end{bmatrix}\dot{A}_{Tq} \tag{16}$$

In the formula, $A_1 = \frac{2\dot{r}^2-2\dot{r}}{r^2}$, $A_2 = -\frac{2\dot{r}+1}{r}$, $B = \frac{1}{r\tau}$ and $C = \frac{1}{r}$.

In order to ensure that the LOS angle rate can quickly converge to zero when considering the first-order dynamic characteristics of the autopilot and infrared interference, the non-singular terminal sliding mode is selected for the time-varying linear uncertain system (16) as follows:

$$S = x_1 + \beta x_2^{\gamma} \tag{17}$$

where $\beta > 0$, $1 < \gamma < 2$, $\gamma = \frac{a}{b}$, a and b are positive odd numbers.

By differentiating the sliding mode Equation (17), the following can be obtained as follows:

$$\dot{S} = \dot{x}_1 + \beta\gamma x_2^{\gamma-1}\dot{x}_2 \tag{18}$$

By substituting the Guidance Equation (16) into Equation (18), the following can be obtained as follows:

$$\dot{S} = x_2 + \beta\gamma x_2^{\gamma-1}(A_1x_1 + A_2x_2 + BA_{Mq} - BA_{Mc} + C\dot{A}_{Tq}) \tag{19}$$

According to Lemma 1, it can be concluded that the sufficient condition for the finite-time convergence of the Sliding Mode Equation (17) is to design A_{Mc} such that:

$$S[\dot{S} + \beta\gamma x_2^{\gamma-1}\beta_1|S|^{\eta}\mathrm{sgn}S] \le 0 \tag{20}$$

where $\beta_1 = const > 0$, $-1 < \eta = const < 1$.

Proof. Choose a smooth positive definite function

$$V = S^2 \tag{21}$$

By differentiating the V, the following can be obtained:

$$\dot{V} = 2S\dot{S} \le -2\beta\gamma x_2^{\gamma-1}\beta_1|S|^{\eta+1} = -2\beta\gamma\beta_1 x_2^{\gamma-1}V^{\frac{\eta+1}{2}} \tag{22}$$

Let $\phi(x_2) = -2\beta\gamma\beta_1 x_2^{\gamma-1}$, both a and b are positive odd numbers and $1 < \gamma < 2$. Therefore, $\gamma - 1 = \frac{a-b}{b}$ can be obtained, since $1 < \gamma < 2$ can explain $a > b$. Both a and b are positive odd numbers, so $a - b$ is a positive even number. Thus, when $x_2 \neq 0$, $x_2^{\gamma-1} > 0$, in which case there is $\phi(x_2) < 0$, the system satisfies the Lyapunov stability principle. In the guidance process, there exists a sufficiently small positive number ω satisfying $\omega \le x_2^{\gamma-1}$, which can be obtained from Equation (22) as follows:

$$\dot{V} \le -2\beta\gamma\beta_1 x_2^{\gamma-1}V^{\frac{\eta+1}{2}} \le -2\beta\gamma\beta_1\omega V^{\frac{\eta+1}{2}} \tag{23}$$

According to Lemma 1, the sliding mode S converges to zero in finite time, and the finite-time t_{e1} satisfies:

$$t_{e1} < \frac{|S(0)|^{\frac{1-\eta}{2}}}{\beta\gamma\beta_1\omega(1-\eta)} \tag{24}$$

In the formula, $S(0) = x_1(0) + \beta x_2(0)^\gamma$. It can be seen from the Equation (24) that when β_1 is larger, the convergence rate is faster. □

Thus, it is proved that the Sliding Mode Equation (17) can be convergent in a finite-time by designing A_{Mc}. By substituting Equation (19) into Equation (20), we can obtain:

$$\begin{aligned} &S[\dot{S} + \beta\gamma x_2^{\gamma-1}\beta_1|S|^\eta \mathrm{sgn}S] \\ &= S[x_2 + \beta\gamma x_2^{\gamma-1}(A_1x_1 + A_2x_2 + BA_{Mq} - BA_{Mc} + C\dot{A}_{Tq}) + \beta\gamma x_2^{\gamma-1}\beta_1|S|^\eta \mathrm{sgn}S] \le 0 \end{aligned} \tag{25}$$

The guidance law is designed as follows:

$$A_{Mc} = \frac{A_1x_1 + A_2x_2 + BA_{Mq} + \frac{1}{\beta\gamma}x_2^{2-\gamma} + \frac{1}{\beta\gamma}kSx_2^{1-\gamma} + \beta_1|S|^\eta \mathrm{sgn}S + C\dot{A}_{Tq}}{B} \tag{26}$$

3.2. Proof of Finite-Time Convergence

The design of A_{Mc} can make the sliding mode S converge in finite time, and the convergence time satisfies Equation (24). When the sliding mode S converges to zero, it can be obtained from Equation (17) and on the sliding mode:

$$x_1 + \beta x_2^\gamma = 0 \tag{27}$$

We define the Lyapunov function as follows:

$$V_1 = x_1^2 \tag{28}$$

Taking the derivative of V_1, the following can be obtained:

$$\dot{V}_1 = 2x_1\dot{x}_1 = 2x_1x_2 = -2\left(\frac{1}{\beta}\right)^{\frac{1}{\gamma}} V_1^{\frac{\gamma+1}{2\gamma}} \tag{29}$$

According to Lemma 1, the guidance system state x_1 converges to zero in finite time on the sliding mode and the LOS angle rate $\dot{q}$ converges to zero in finite time. According to Lemma 1, the convergence time is as follows:

$$t_{e2} = \frac{2\gamma\beta^{\frac{1}{\gamma}}|x_1(t_{e1})|^{\frac{\gamma-1}{2\gamma}}}{\gamma-1} \tag{30}$$

Therefore, the total convergence time of the guidance system satisfies:

$$t_e = t_{e1} + t_{e2} \le \frac{|S(0)|^{\frac{1-\eta}{2}}}{\beta\gamma\beta_1\omega(1-\eta)} + \frac{2\gamma\beta^{\frac{1}{\gamma}}|x_1(t_{e1})|^{\frac{\gamma-1}{2\gamma}}}{\gamma-1} \tag{31}$$

3.3. Design of FTCG Based on FTDO

The LOS angle acceleration x_2 is required in both the Sliding Mode Equation (17) and the Guidance Law Equation (26), and x_2 can be replaced by Equation (11). In the actual process of terminal guidance, target acceleration is not available. But target maneuvering acceleration is usually bounded and satisfies $\left|\dot{A}_{Tq}\right| \le L$, where constant $L > 0$. Therefore, the FTDO [7] is used to estimate the maneuvering acceleration of the target:

$$\begin{cases} x_3 = r\dot{q} \\ \dot{x}_3 = -\frac{\dot{r}}{r}x_3 + A_{Tq} - A_{Mq} \\ \dot{z}_0 = v_0 - \frac{\dot{r}}{r}x_3 - A_{Mq} \\ v_0 = -\lambda_0|z_0 - x_3|^{\frac{1}{2}}\operatorname{sgn}(z_0 - x_3) + z_1 \\ \dot{z}_1 = v_1 \\ v_1 = -\lambda_1\operatorname{sgn}(z_1 - v_0) \end{cases} \tag{32}$$

where λ_0 and λ_1 are sufficiently large positive constants, z_0 and z_1 respectively can exactly estimate x_3 and A_{Tq} in finite time. Therefore, x_2 can be estimated by the following equation:

$$\hat{x}_2 = -\frac{2\dot{r}}{r}\dot{q} - \frac{1}{r}A_{Mq} + \frac{1}{r}z_1 \tag{33}$$

where $\hat{x}_2$ is the estimate of x_2. The sliding mode S can be estimated by the following formula:

$$\hat{S} = x_1 + \beta\hat{x}_2^{\gamma} \tag{34}$$

where $\hat{S}$ is the estimate of S.

Thus, Equation (26) can be expressed as follows:

$$A_{Mc} = \frac{A_1x_1 + A_2\hat{x}_2 + BA_{Mq} + \frac{1}{\beta\gamma}\hat{x}_2^{2-\gamma} + \frac{1}{\beta\gamma}k\hat{S}\hat{x}_2^{1-\gamma} + \beta_1\left|\hat{S}\right|^{\eta}\operatorname{sgn}\hat{S} + C\dot{A}_{Tq}}{B} \tag{35}$$

In the formula, $\dot{A}_{Tq}$ is difficult to obtain but $\dot{A}_{Tq}$ is a small quantity compared to A_{Tq} in a guidance cycle and it can be compensated for by variable structure terms. Therefore, A_M can be expressed as:

$$A_M = \frac{A_1x_1 + A_2\hat{x}_2 + BA_{Mq} + \frac{1}{\beta\gamma}\hat{x}_2^{2-\gamma} + \frac{1}{\beta\gamma}k\hat{S}\hat{x}_2^{1-\gamma} + \beta_1\left|\hat{S}\right|^{\eta}\operatorname{sgn}\hat{S}}{B\cos(q - \theta_M)} \tag{36}$$

4. Simulation Results and Analysis

According to Equation (36) of the guidance law, the guidance law has a variable structure term which contains the switching function term $\operatorname{sgn}(\hat{S})$ and the control quantity needs to be switched constantly. But due to the limited calculation delay and switching speed of the control system, the jitter of the actuator will be caused. This jitter is the jitter of the flight vehicle body. If the jitter is too large, the flight vehicle will lose stability and affect the accuracy of hitting the target. In order to reduce the jitter and smooth the switching function in the above guidance law, a saturation function $sat_{\delta}(x)$ can be used to replace the switching function $\operatorname{sgn}(\hat{S})$. The expression of the saturation function is shown as follows:

$$sat_{\delta}(\hat{S}) = \begin{cases} 1, \hat{S} > \delta \\ \hat{S}/\delta, \left|\hat{S}\right| \le \delta \\ -1, \hat{S} < -\delta \end{cases} \tag{37}$$

There is also a switching function in Equation (32) of the finite-time disturbance observer, and the saturation functions $\frac{z_0 - x_3}{|z_0 - x_3| + d}$ and $\frac{z_1 - v_0}{|z_1 - v_0| + d}$ are used to replace the switching function in Equation (32) in order to reduce the observer jitter.

In order to verify the applicability of the guidance law in the complex adversarial scenarios, the interception simulation is carried out on the targets in multiple environments. The set parameters of flight vehicle, target, infrared decoy, finite-time convergent disturbance observer, and guidance law are shown in Tables 1–3:

Table 1. Related parameters values of the flight vehicle and target.

$(X_{M0}, Y_{M0})/m$	$(X_{T0}, Y_{T0})/\mathrm{m}$	$V_M/(\mathrm{m \cdot s^{-1}})$	$V_T/(\mathrm{m \cdot s^{-1}})$
(0,1000)	(7000,3000)	1000	600
$\theta_{M0}/(°)$	$\theta_{T0}/(°)$	$A_M\|_{\max}/\mathrm{g}$	
0	0	±40	

Table 2. Related parameters values of the infrared decoy.

m_{H0}/kg	$\dot{m}_H/(\mathrm{kg \cdot s^{-1}})$	S/m^2	C_H
0.25	0.03	0.0032	0.3
K	n		
2	1		

Table 3. Related parameters values of the finite-time disturbance observer and guidance law.

λ_0	λ_1	d	k	β
15	35	0.001	1	1
β_1	η	γ	δ	
10	0.1	5/3	0.001	

The constant time of the flight vehicle's autopilot is $\tau = 0.3$ and the recognition time of the flight vehicle seeker is 0.1 s. The burning time of the infrared decoy is 1 s. The initial velocity V_{H0} of the infrared decoy is the same as the velocity of the target at the moment it is released. Therefore, V_{Hx0} and V_{Hy0} have the same components in the X and Y directions as the target's velocity at the time of release. The gravitational acceleration is taken as $g = 9.8\ \mathrm{m/s^2}$ and the air density as $\rho = 1.29\ \mathrm{kg/m^3}$.

In order to fully verify the robustness of the guidance law, it is assumed that the target can take two different maneuvers and release infrared decoys with a different remaining time t_{go} to evade the flight vehicle:

(1) Scenario 1: The target undertakes a constant maneuver $A_T = 5g$ and releases an infrared decoy when the remaining time is $t_{go} = 1$ s or $t_{go} = 2$ s.

(2) Scenario 2: The target undertakes a sinusoidal maneuver $A_T = 5g\sin(0.2\pi t)$ and releases an infrared decoy when the remaining time is $t_{go} = 1$ s or $t_{go} = 2$ s.

(3) Scenario 3: The target undertakes a constant maneuver $A_T = 5g$ and respectively releases an infrared decoy once when the remaining time is $t_{go} = 1.4$ s and $t_{go} = 2$ s. The interval between the two releases of the infrared decoy is 0.6 s.

(4) Scenario 4: The target undertakes a sinusoidal maneuver $A_T = 5g\sin(0.2\pi t)$ and respectively releases an infrared decoy once when the remaining time is $t_{go} = 1.4$ s and $t_{go} = 2$ s. The interval between the two releases of the infrared decoy is 0.6 s.

For these four different complex adversarial scenarios, the simulation results obtained using the guidance law (36) are shown in Figures 3–5. Figure 3 represents the simulation results for Scenario 1, Figure 4 represents the simulation results for Scenario 2, Figure 5 represents the simulation results for Scenario 3 and Scenario 4. Table 4 shows the miss distance, strike time, and convergence time in the above scenario.

The proposed FTCG can accurately strike the target in the scenarios of infrared interference, as shown in Figures 3a and 4a. The validation results in Table 4 indicate that the miss distance is only 0.1560 m when the remaining time is $t_{go} = 1$ s and it is only 0.1423 m when the remaining time is $t_{go} = 2$ s in Scenario 1. In Scenario 2, the miss distance is only 0.3018 m when the remaining time is $t_{go} = 1$ s, and it is only 0.3029 m when the remaining time is $t_{go} = 2$ s. This illustrates the good accuracy of the FTCG in complex adversarial scenarios. Figures 3b and 4b show that the infrared decoy has a significant impact on the LOS angle rate, and the impact becomes greater as the remaining time decreases. However, the FTCG can quickly converge the LOS angle rate to 0 rad/s after the disturbance and Table 4 shows that the LOS angle rate can converge to 0 rad/s for about 0.4 s after disturbance, enhancing the guidance stability and demonstrating the good robustness of the FTCG in complex adversarial scenarios. Figures 3c and 4c show that FTCG experiences overload saturation at the initial stage of terminal guidance, indicating the maximum utilization of the flight vehicle's overload capacity during this period. Figures 3d and 4d show that the infrared decoy also has a considerable impact on the observer. However, the FTDO accurately estimates and compensates for the target maneuver in the guidance law in a limited time after the disturbance, showcasing the good robustness of the FTDO in complex adversarial scenarios.

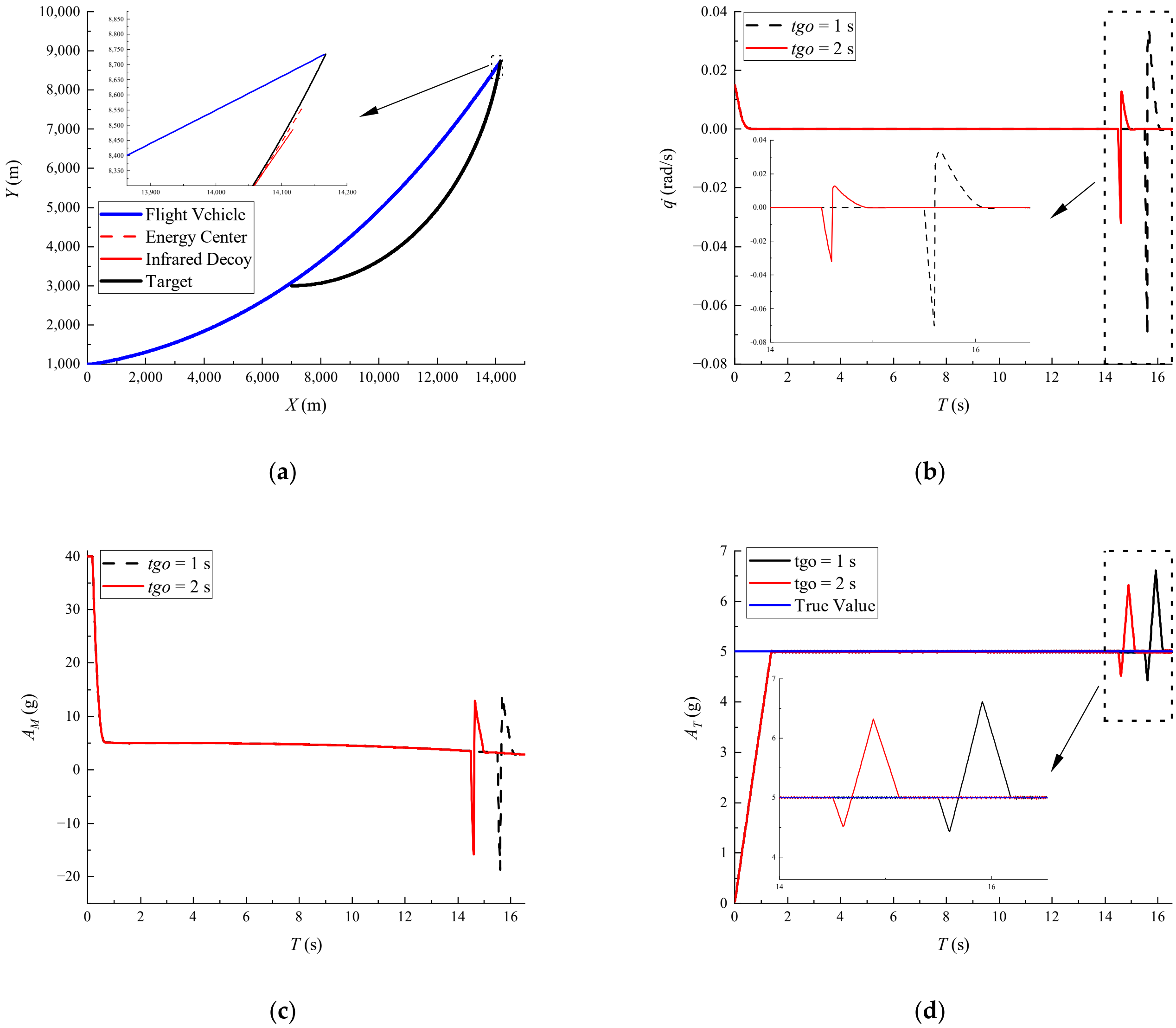

Figure 3. Simulation results of Scenario 1. (**a**) Trajectory of motion when $t_{go} = 1$ s; (**b**) Change curve of the LOS angle rate; (**c**) Change curve of the flight vehicle normal overload; (**d**) Estimation result of target acceleration.

The FTCG can rapidly converge the LOS angle rate to 0 rad/s in both Scenario 3 and Scenario 4, as shown in Figure 5a. According to Table 4, the miss distance is only 0.0457 m in Scenario 3 and 0.2884 m in Scenario 4, indicating that the FTCG exhibits a good accuracy in the aforementioned scenarios. Figure 5b illustrates that the FTDO also accurately estimates and compensates for target maneuvers within a finite time even under disturbances, demonstrating its good robustness in the aforementioned scenarios.

Table 4. Miss distance, strike time, and convergence time of four scenarios.

	Miss Distance/m	Strike Time/s	Convergence Time/s
Scenario 1 ($t_{go} = 1$ s)	0.1560	16.5280	about 0.432
Scenario 1 ($t_{go} = 2$ s)	0.1423	16.5280	about 0.387
Scenario 2 ($t_{go} = 1$ s)	0.3018	18.0590	about 0.306
Scenario 2 ($t_{go} = 2$ s)	0.3029	18.0590	about 0.450
Scenario 3	0.0457	16.5280	about 0.387/0.468
Scenario 4	0.2884	18.0590	about 0.378/0.306

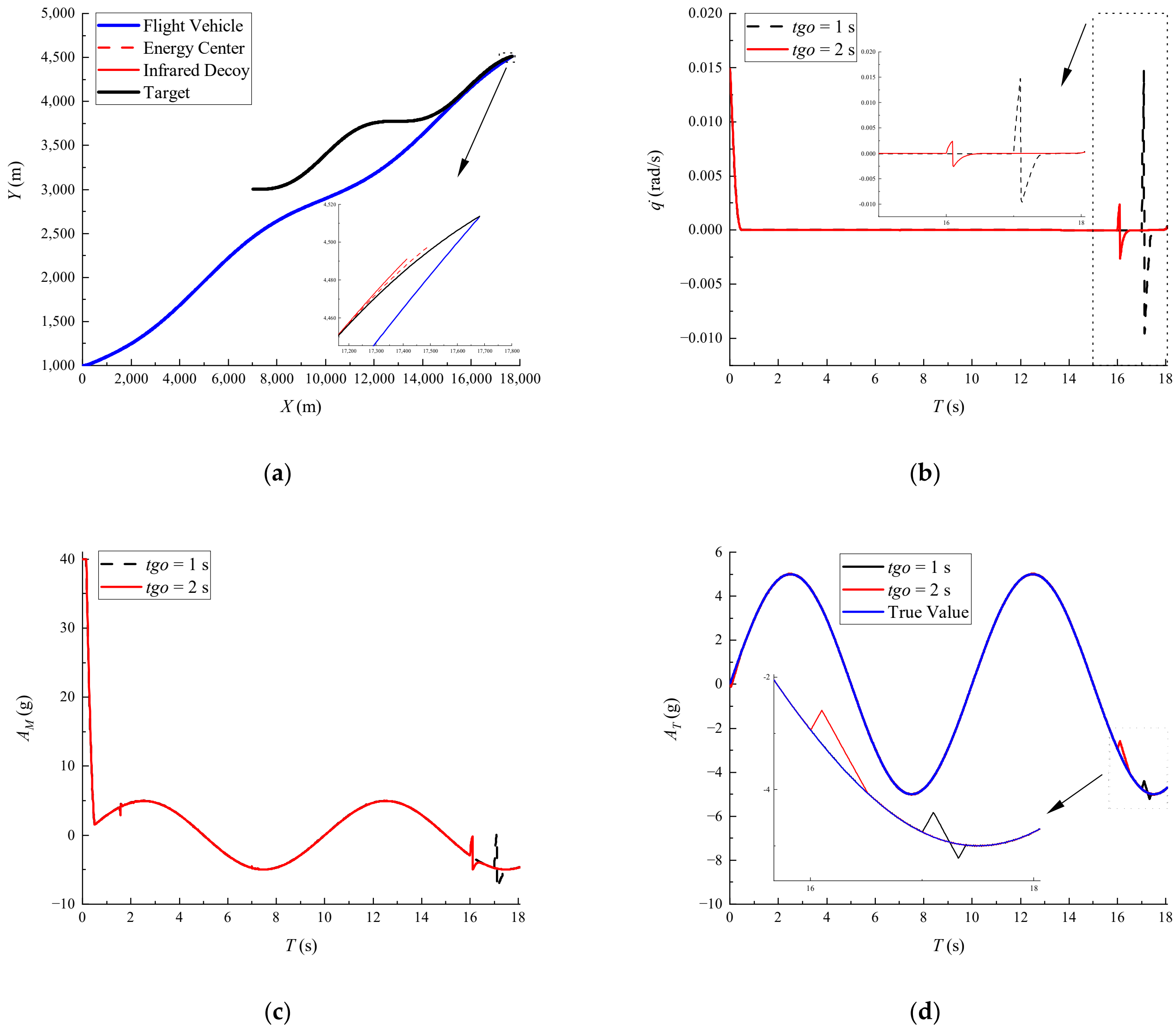

Figure 4. Simulation results of Scenario 2. (**a**) Trajectory of motion when $t_{go} = 1$ s; (**b**) Change curve of the LOS angle rate; (**c**) Change curve of the flight vehicle normal overload; (**d**) Estimation result of target acceleration.

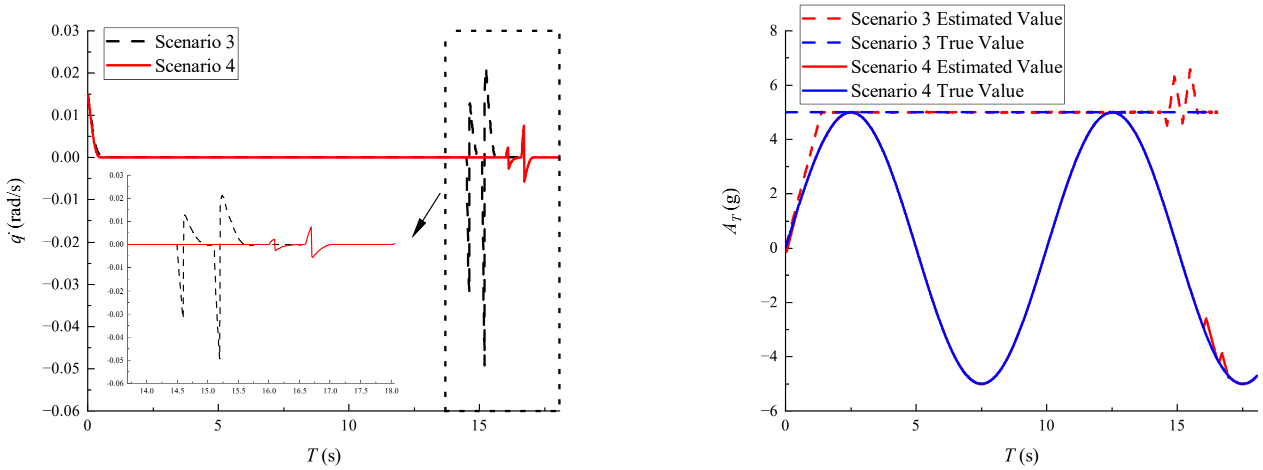

(**a**) (**b**)

Figure 5. Simulation results of Scenario 3 and Scenario 4. (**a**) Change curve of the LOS angle rate; (**b**) Estimation result of target acceleration.

The above target maneuver is merely a simple maneuver using a certain constant value. In order to further illustrate the performance of the FTCG, it will be validated through simulation in Scenario 5. The target maneuver is characterized by the following random movements:

$$A_T = \begin{cases} 5g & T \leq 2\text{ s} \\ -3g & 2\text{ s}<T \leq 5\text{ s} \\ 5g & 5\text{ s}<T \leq 11\text{ s} \\ -5g & 11\text{ s}<T \end{cases} \tag{38}$$

Six sets of infrared decoys will be released with a 0.6 s release interval. Each release comprises 10 infrared decoys and denoted as $n = 10$. The simulation results are illustrated in Figure 6:

When the target is undergoing irregular acceleration motion, it can be seen from Figure 6a that the FTCG can accurately strike the target in Scenario 5. The miss distance is only 0.1152 m, indicating that the FTCG still maintains a good accuracy in more complex adversarial scenarios. From Figure 6b, it can be observed that the infrared decoy has a significant impact on the LOS angle rate, the effect is greater as the remaining time decreases. The LOS angle rate can converge to zero after being disturbed for approximately 0.37 s. The FTDO can quickly catch up with the target's overload after the target's acceleration has changed. It also accurately estimates the target's overload after being disturbed and compensates for the target's overload to the guidance law.

In order to further illustrate the advantages of the guidance law (36), a comparative simulation verification is conducted with the SMGL and the ASMGL based on ESO.

The SMGL is defined as follows:

$$A_M = \frac{k_1|\dot{r}|x_1 + \varepsilon_1 \text{sgn}(x_1)}{\cos(q - \theta_M)} \tag{39}$$

$\frac{x_1}{|x_1|+\delta_1}$ is used to replace the switching function of Equation (39) and let the guidance law parameters $k_1 = 3$, $\varepsilon_1 = 100$, $\delta_1 = 0.001$.

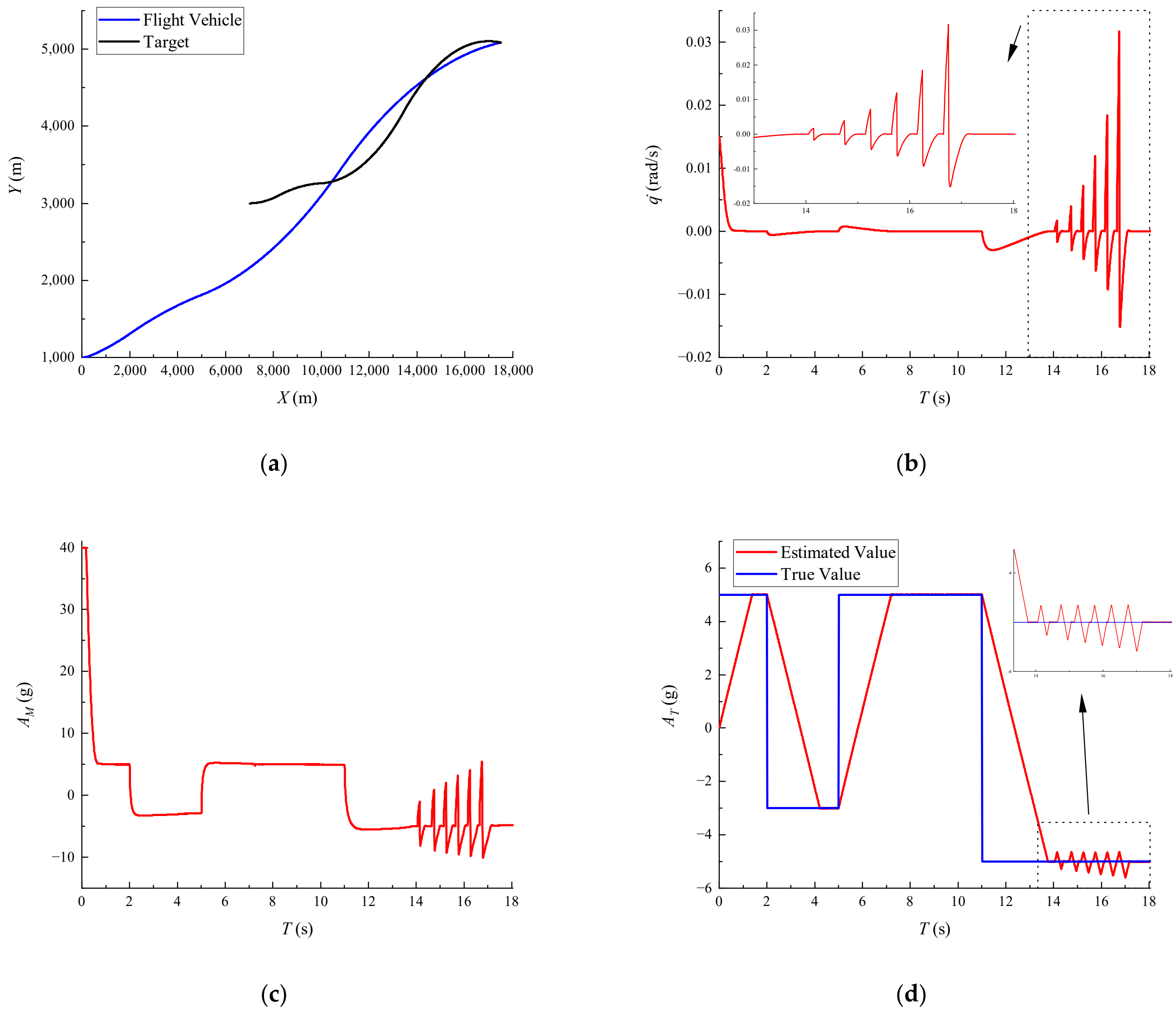

Figure 6. Simulation results of Scenario 5. (**a**) Trajectory of motion; (**b**) Change curve of the LOS angle rate; (**c**) Change curve of the flight vehicle normal overload; (**d**) Estimation result of target acceleration.

The ASMGL is defined as follows:

$$A_M = \frac{(A_1 + k_2 k_3 \frac{|\dot{r}|}{r})x_1 + (A_2 + k_2 + k_3 \frac{|\dot{r}|}{r})\hat{x}_2 + BA_{Mq} + \frac{\varepsilon_2}{r}\mathrm{sgn}(\hat{S}_1)}{B\cos(q - \theta_M)} \tag{40}$$

where:

$$\begin{cases} \hat{S}_1 = k_2 x_1 + \hat{x}_2 \\ \hat{x}_2 = -\frac{2\dot{r}}{r}\dot{q} - \frac{1}{r}A_{Mq} + \frac{1}{r}z_3 \end{cases} \tag{41}$$

where z_3 is the output of the ESO Equation (42):

$$\begin{cases} e_1 = z_2 - x_1 \\ \dot{z}_2 = \frac{z_3}{r} - \beta_{01}e_1 - 2\frac{\dot{r}}{r}\dot{q} - \frac{1}{r}A_{Mq} \\ \dot{z}_3 = -\beta_{02}fal(e_1, m, n) \end{cases} \tag{42}$$

The function $fal(e_1, m, n)$ is defined as follows:

$$fal(e_1, m, n) = \begin{cases} |e_1|^m \mathrm{sgn}(e_1), |e_1| > n \\ \frac{e_1}{n^{1-m}}, |e_1| \le n \end{cases} \tag{43}$$

where e_1 is the error between the estimate of the observer and the true value, z_2 and z_3 respectively are the estimates of $\dot{q}$ and A_{Tq}, $\frac{\hat{S}_1}{|\hat{S}_1|+\delta_2}$ is used to replace the switching function of Equation (40) in order to reduce vibration. Let the guidance law parameters $k_2 = 2$, $k_3 = 3$, $\varepsilon_2 = 50$, $\delta_2 = 0.01$ and the observer parameters $\beta_{01} = 1000$, β_{02} = 30,000, $m = 0.1$, $n = 0.001$. The three guidance laws are compared and simulated in Scenario 6, where the target undertakes a constant maneuver for $A_T = 5$ g. When the remaining time is $t_{go} = 2$ s, the decoy is released once, the impact time is 0.3 s, and the second decoy is released when the impact is 0.5 s past. The simulation results are shown in Figure 7. Table 5 shows the miss distance, strike time, and convergence time of the three guidance laws.

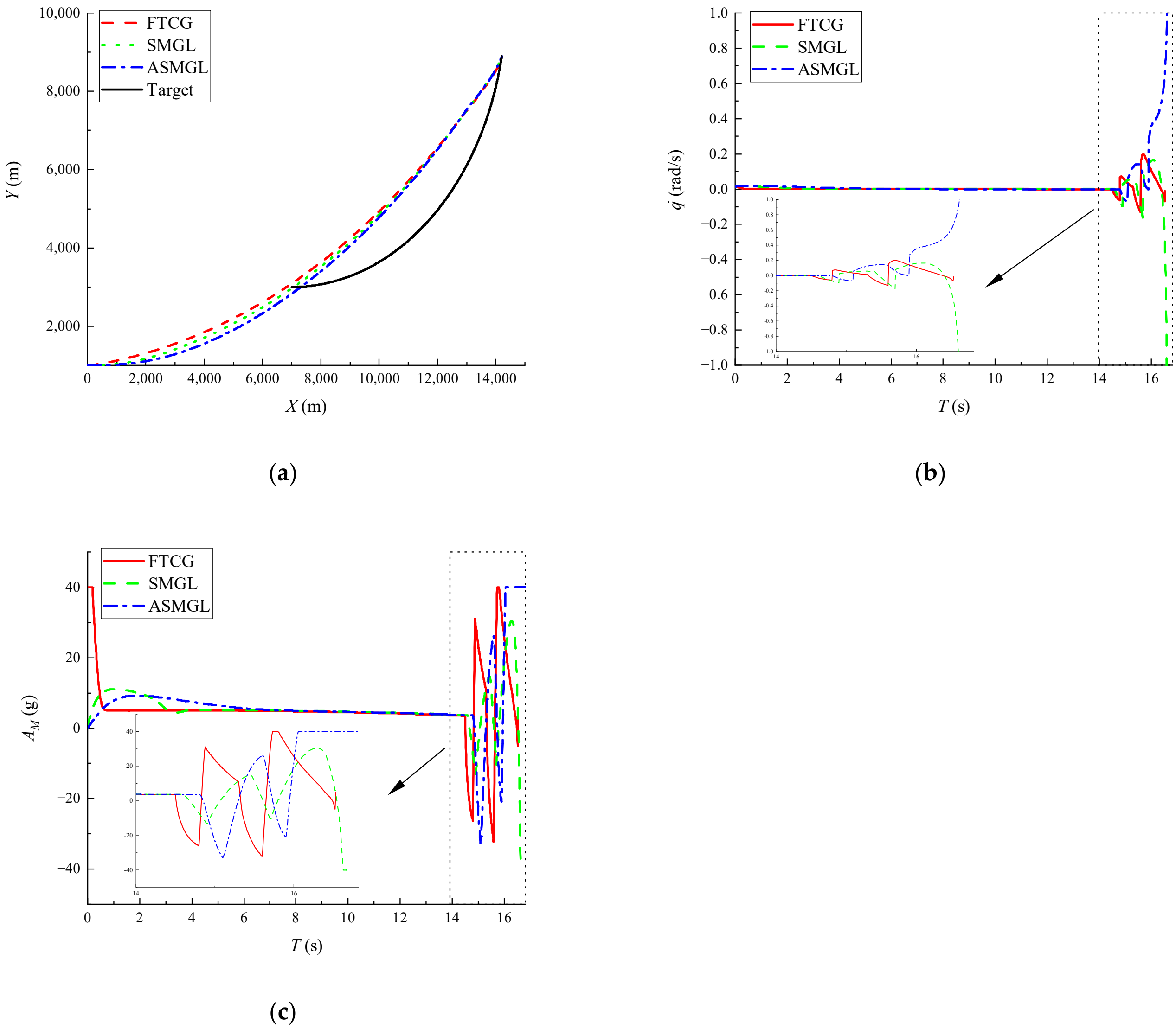

Figure 7. Simulation results of the three guidance laws. (**a**) Trajectory of motion; (**b**) Change curve of the LOS angle rate; (**c**) Change curve of the flight vehicle normal overload.

Table 5. Miss distance, strike time, and convergence time under the guidance of the three guidance laws.

Guidance Law	Miss Distance/m	Strike Time/s	Convergence Time/s
FTCG	0.1775	16.5350	about 0.927
SMGL	2.1567	16.6750	failure to converge
ASMGL	12.0415	16.8190	failure to converge

From Figure 7a, it can be seen that the FTCG, ASMGL, and SMGL are all pursuing the target. However, it can be seen from Table 5 that the miss distance of the FTCG is only 0.1775 m, while the miss distance of the SMGL and ASMGL is as high as 2.1567 m and 12.0415 m, indicating that the FTCG has a better accuracy than the SMGL and ASMGL. From Figure 7b, it can be seen that after being disturbed, the LOS angle rate of the FTCG rapidly converges to 0 rad/s, and the convergence time is about 0.837 s. However, the LOS angle rate of the SMGL and ASMGL diverges and does not converge to 0 rad/s. From Figure 7c, it can be observed that the FTCG experiences overload saturation in the early terminal guidance phase, indicating that the flight vehicle's overload capability is maximally utilized during this period, with a smaller overload in the later phase to improve the flight vehicle stability. On the other hand, the ASMGL and SMGL have a lower overload in the early terminal guidance phase and require higher overload or even saturation at the end, which is not conducive to a stable flight vehicle performance and is not practical in practice.

The above simulation cases illustrate the effectiveness of the FTCG in a two-dimensional longitudinal plane. Following this, the FTCG will be extended to a three-dimensional coordinate system which is typically divided into the pitch plane and horizontal plane for analysis. Without considering the dynamic characteristics, the guidance equations for the pitch plane and the horizontal plane are as follows:

$$\begin{cases} \ddot{q}_\varepsilon = -\frac{2\dot{r}}{r}\dot{q}_\varepsilon - \dot{q}_\beta^2 \sin q_\varepsilon \cos q_\varepsilon - \frac{A_{M\varepsilon}}{r} + \frac{A_{T\varepsilon}}{r} \\ \ddot{q}_\beta = -\frac{2\dot{r}}{r}\dot{q}_\beta - 2\dot{q}_\varepsilon \dot{q}_\beta \tan q_\varepsilon - \frac{A_{M\beta}}{r\cos q_\varepsilon} + \frac{A_{T\beta}}{r\cos q_\varepsilon} \end{cases} \tag{44}$$

where q_ε and q_β are the LOS angles of the pitch plane and the horizontal plane, $A_{M\varepsilon}$ and $A_{M\beta}$ are the normal acceleration of the flight vehicle in the pitch plane and the horizontal plane, and $A_{T\varepsilon}$ and $A_{T\beta}$ are the normal acceleration of the target in the pitch plane and the horizontal plane. Ignoring the higher-order terms in the above equation, Equation (44) is simplified as follows:

$$\begin{cases} \ddot{q}_\varepsilon = -\frac{2\dot{r}}{r}\dot{q}_\varepsilon - \frac{A_{M\varepsilon}}{r} + \frac{A_{T\varepsilon}}{r} \\ \ddot{q}_\beta = -\frac{2\dot{r}}{r}\dot{q}_\beta - \frac{A_{M\beta}}{r\cos q_\varepsilon} + \frac{A_{T\beta}}{r\cos q_\varepsilon} \end{cases} \tag{45}$$

In order to illustrate the advantages of this guidance law in the three-dimensional coordinate system, the PNG, which is most commonly used by the flight vehicle is used to compare with the FTCG. The PNG is in the following form:

$$\begin{cases} A_{M\varepsilon} = N\dot{r}\dot{q}_\varepsilon \\ A_{M\beta} = N\dot{r}\dot{q}_\beta \cos q_\varepsilon \end{cases} \tag{46}$$

where the guidance coefficient is $N = 3$. The FTCG is in the following form:

$$\begin{cases} A_{M\varepsilon} = \frac{A_1 x_{1\varepsilon} + A_2 \hat{x}_{2\varepsilon} + BA_{M\varepsilon} + \frac{1}{\beta\gamma}\hat{x}_{2\varepsilon}^{2-\gamma} + \frac{1}{\beta\gamma}k\hat{S}_\varepsilon \hat{x}_{2\varepsilon}^{1-\gamma} + \beta_1 |\hat{S}_\varepsilon|^\eta \operatorname{sgn}\hat{S}_\varepsilon}{B\cos(q_\varepsilon - \theta_{M\varepsilon})} \\ A_{M\beta} = \frac{(A_1 x_{1\beta} + A_2 \hat{x}_{2\beta} + BA_{M\beta} + \frac{1}{\beta\gamma}\hat{x}_{2\beta}^{2-\gamma} + \frac{1}{\beta\gamma}k\hat{S}_\beta \hat{x}_{2\beta}^{1-\gamma} + \beta_1 |\hat{S}_\beta|^\eta \operatorname{sgn}\hat{S}_\beta)\cos q_\varepsilon}{B\cos(q_\beta - \theta_{M\beta})} \end{cases} \tag{47}$$

where $x_{1\varepsilon}$ and $x_{1\beta}$ respectively represent the LOS angle rate $\dot{q}_\varepsilon$ in the pitch plane and $\dot{q}_\beta$ in the horizontal plane, $\hat{x}_{2\varepsilon}$ and $\hat{x}_{2\beta}$ respectively represent the estimated value of the LOS angle acceleration $\ddot{q}_\varepsilon$ in the pitch plane and $\ddot{q}_\beta$ in the horizontal plane, $\hat{S}_\varepsilon$ and $\hat{S}_\beta$ respectively represent the estimated value of sliding mode in the pitch plane and in the horizontal plane, $\theta_{M\varepsilon}$ and $\theta_{M\beta}$ respectively represent the pitch angle and roll angle of the flight vehicle; the parameter values of the FTCG have been given in Table 3. At this time, the initial parameters of the flight vehicle and the target are shown in Table 6:

Table 6. Related parameters values of the flight vehicle and target.

$(X_{M0}, Y_{M0}, Z_{M0})/\mathrm{m}$	$(X_{T0}, Y_{T0}, Z_{M0})/\mathrm{m}$	$V_M/(\mathrm{m}\cdot\mathrm{s}^{-1})$	$V_T/(\mathrm{m}\cdot\mathrm{s}^{-1})$
(1000,0,1000)	(7000,3000,3000)	1000	600
$\theta_{M\varepsilon}/(^\circ)$	$\theta_{M\beta}/(^\circ)$	$\theta_{T\varepsilon}/(^\circ)$	$\theta_{T\beta}/(^\circ)$
0	0	0	0

The target adopts the random maneuver shown in Equation (38) in both the pitch plane and the horizontal plane. The infrared decoy is released when $t_{go} = 1$ s and its parameters are given in Table 2. In order to be closer to the real scenario, the flight vehicle has a guidance blind area of 200 m. The flight vehicle will fly according to the acceleration before entering the blind area until the end of the simulation. The simulation results are shown in Figure 8 and Table 7:

Table 7. Simulation result of three-dimensional coordinate system.

Guidance Law	Miss Distance/m	Strike Time/s
FTCG	0.2481	15.80
PNG	3.5170	16.5470

As shown in Figure 8a, it can be seen in the three-dimensional coordinate system that both the FTCG and PNG are pursuing the target. However, it can be seen from Table 7 that the miss distance of the FTCG is only 0.2481 m, while the miss distance of the PNG is as high as 3.5170 m, indicating that the FTCG is also effective in a three-dimensional coordinate system. From Figure 8b,c, it can be seen that before entering the blind area, $\dot{q}_\varepsilon$ and $\dot{q}_\beta$ rapidly converge to 0 rad/s after the FTCG experiences interference and finally converge to 1.46×10^{-4} rad/s and 1.25×10^{-4} rad/s. In the blind area, the target is attacked with the attitude of an almost constant LOS angle and the local quasi-parallel approach is realized. However, $\dot{q}_\varepsilon$ and $\dot{q}_\beta$ cannot converge to 0 rad/s after the PNG experiences interference and finally converges to 6.13×10^{-2} rad/s and 2.27×10^{-1} rad/s. Therefore, the quasi-parallel approach cannot be achieved in the blind area, resulting in a large miss distance. From Figure 8d,e, it can be seen that in the initial stage of final guidance, the FTCG experiences overload saturation in both the pitch plane and the horizontal plane, indicating that the flight vehicle's overload capability has been utilized to the maximum extent during this period. In the final stage, the overload is small and the flight vehicle has a good stability. However, the PNG has a small overload in the initial stage of final guidance and a large required overload at the end. This is not conducive to the stability of the flight vehicle. Therefore, it can be shown that the FTCG also has a good effectiveness in three-dimensional space.

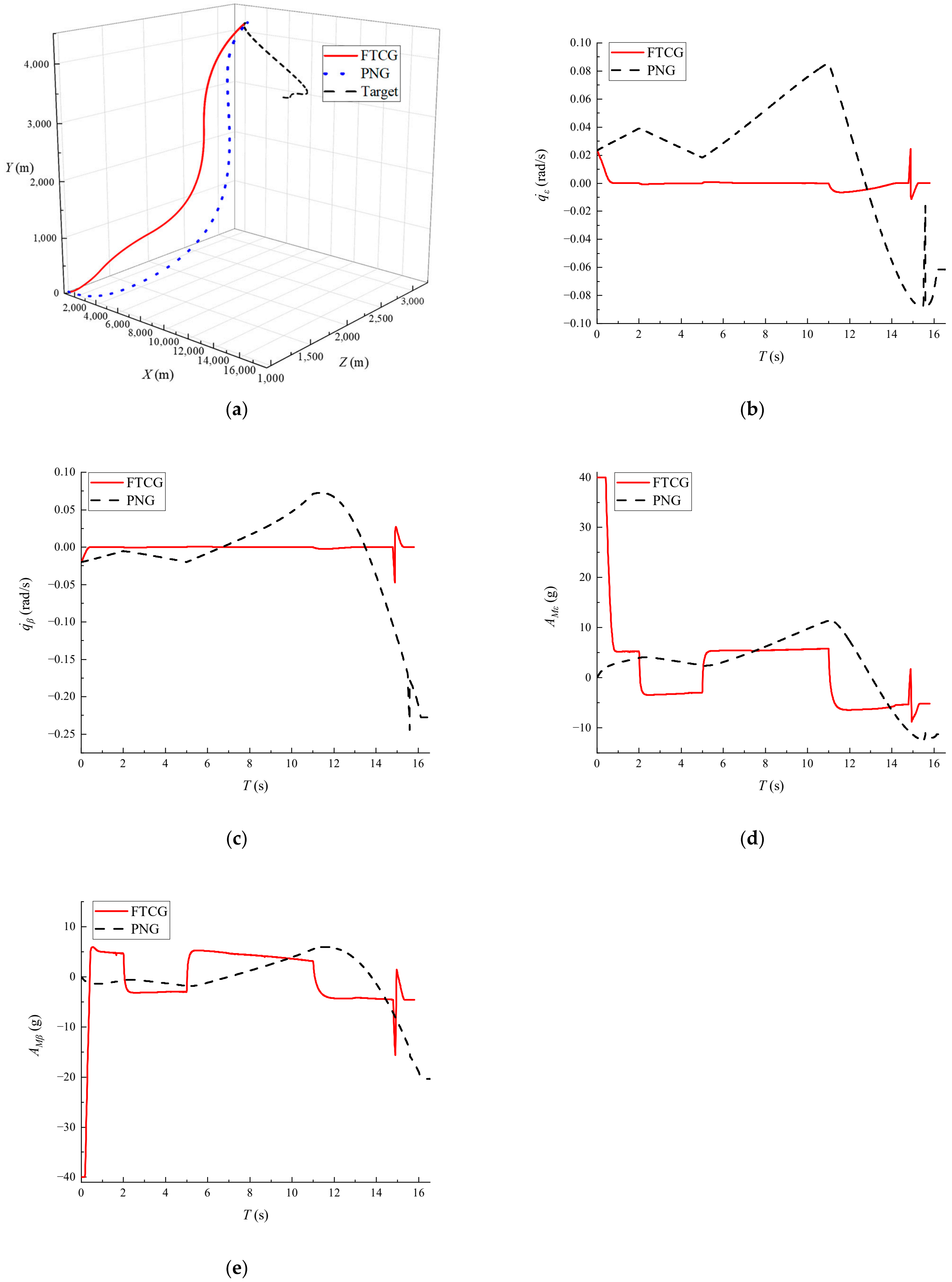

Figure 8. Simulation results of three-dimensional coordinate system. (**a**) Trajectory of motion; (**b**) Change curve of the LOS angle rate in the pitch plane; (**c**) Change curve of the LOS angle rate in the horizontal plane. (**d**) Change curve of the flight vehicle normal overload in the pitch plane. (**e**) Change curve of the flight vehicle normal overload in the horizontal plane.

5. Conclusions

This article proposes an FTCG based on the FTDO which improves the flight vehicle accurate strike capability in complex adversarial scenarios. Based on the influence mechanism of an infrared decoy on the flight vehicle, the relative motion model between the flight vehicle and the target is established, as well as the motion model of the infrared decoy. According to the principle of centroid interference, a motion model for the energy center is established. A complex adversarial scenario consisting of the flight vehicle, target, infrared decoy, and energy center is constructed. In the design process of the guidance law, the first-order dynamic characteristics of the autopilot are taken into consideration. The finite-time control theory is used to design the terminal guidance law and the convergence time of the guidance law is derived to provide guidance for parameter selection. In the case where the target acceleration is unmeasurable, an FTDO is used to estimate the target acceleration and compensate for it in the guidance law, improving the accuracy of the terminal guidance law. The simulation results indicate that under various complex adversarial scenarios, the LOS angle rate can quickly converge to 0 rad/s and accurately strike the target after being influenced by infrared interference. The estimated value of the target acceleration also converges rapidly to the actual target acceleration and is compensated for in the guidance law after being influenced by infrared interference. A comparison with the SMGL and ASMGL shows that the proposed guidance law can ensure faster convergence and a smaller miss distance in a complex adversarial scenario. Therefore, this guidance law demonstrates a satisfactory guidance accuracy and robustness in a complex adversarial scenario and has advantages over other guidance laws. Finally, the FTCG is extended to a three-dimensional coordinate system and compared with the PNG to further verify its effectiveness and practicability.

Author Contributions: Conceptualization, H.D., X.L. (Xiao Liang) and C.L.; methodology, H.D., X.L. (Xingcheng Li) and C.L.; software, H.D. and D.W.; validation, H.D. and C.L.; formal analysis, H.D.; investigation, H.D.; resources, H.D.; data curation, H.D.; writing—original draft preparation, H.D.; writing—review and editing, H.D., D.W., C.L., X.L. (Xiao Liang) and X.L. (Xingcheng Li); visualization, H.D.; supervision, C.L.; project administration, C.L. All authors have read and agreed to the published version of the manuscript.

Funding: Beijing Institute of Technology Research Fund Program for Young Scholars.

Data Availability Statement: Data are contained within the article.

Conflicts of Interest: The authors declare no conflicts of interest.

References

1. Zhou, W.W.; Kang, M.L.; Zhou, Z.Q. Research of infrared flares influence mechanism on the imaging guidance missile. *Infrared Laser Eng.* **2019**, *48*, 118–124.
2. Li, Q.C.; Zhu, C.X.; Fan, Y.H.; Wan, S.Z.; Yan, J. Study on infrared air-to-air missile guidance accuracy affected by complicated environment. *J. Northwest. Polytech. Univ.* **2019**, *37*, 457–464. [CrossRef]
3. Huang, H.S.; Tong, Z.X.; Li, J.X.; Wang, C.Z.; Chai, S.J. Functional simulation of infrared air-to-air missiles based on combat assessment. *Infrared Laser Eng.* **2015**, *44*, 803–809.
4. Wang, H.Q.; Fang, Y.W.; Wu, Y.L.; Zeng, X.W. The study of infrared decoy jamming characteristic and simulation. *Fire Control Command Control* **2010**, *35*, 25–28.
5. Zhang, W.J.; FU, S.N.; LI, W.; Xia, Q.L. An impact angle constraint integral sliding mode guidance law for maneuvering targets interception. *J. Syst. Eng. Electron.* **2020**, *31*, 168–184. [CrossRef]
6. Shi, Q.L.; Wang, H.; Cheng, H. Multiple constraints-based adaptive three-dimensional back-stepping sliding mode guidance law against a maneuvering target. *Aerospace* **2022**, *9*, 796. [CrossRef]
7. Zhang, Z.M.; Ma, Q.H.; Chen, Y.; Xu, C.; Wang, S.W. Optimal sliding mode guidance law design for maneuvering targets. *J. Proj. Rocket. Missiles Guid.* **2021**, *41*, 139–144.
8. Yang, F.; Xia, G.Q. A finite-time 3D guidance law based on fixed-time convergence disturbance observer. *Chin. J. Aeronaut.* **2020**, *33*, 1299–1310. [CrossRef]
9. Lei, H.M.; Zhang, X.; Dong, F.Y.; Li, J. Finite time convergent zero-effort miss guidance law. *J. Natl. Univ. Def. Technol.* **2015**, *37*, 136–141.

10. Feng, D.; Ren, H.B.; Jian, J.L.; Ji, Y. Finite time convergent guidance law based on filtering extended state observer. *Flight Dyn.* **2016**, *34*, 62–66.
11. Zhao, S.L.; Chen, W.C.; Yang, L. Optimal guidance law with impact-angle constraint and acceleration limit for exo-atmospheric interception. *Aerospace* **2021**, *8*, 358. [CrossRef]
12. Zhang, B.L.; Zhou, D. Optimal predictive sliding-mode guidance law for intercepting near-space hypersonic maneuvering target. *Chin. J. Aeronaut.* **2022**, *35*, 320–331. [CrossRef]
13. Kim, Y.-W.; Kim, B.; Lee, C.-H.; He, S.M. A unified formulation of optimal guidance-to-collision law for accelerating and decelerating targets. *Chin. J. Aeronaut.* **2022**, *35*, 40–54. [CrossRef]
14. Sun, S.; Zhou, D. A finite time convergent variable structure guidance law. *J. Astronaut.* **2008**, *29*, 1258–1262.
15. Zhang, Y.X.; Sun, M.W.; Chen, Z.Q. Sliding-mode variable structure finite-time convergence guidance law. *Control Theory Appl.* **2012**, *29*, 1413–1418.
16. Zhang, K.; Yang, S.C.; Zhang, K.Q.; Yao, Y.Z.; Chen, P. Finite-time convergent sliding mode guidance law with impact angle constraint. *Electron. Opt. Control* **2017**, *24*, 63–66+81. [CrossRef]
17. Zhang, J.; Yang, X.; Liu, Y.X. Guidance law with impact angle constraints based on extended disturbance observer. *J. Beijing Univ. Aeronaut. Astronaut.* **2015**, *41*, 2256–2268.
18. Zhang, W.J.; Lu, T.Y.; Xia, Q.L. Anti-early-warning airplane sliding mode guidance law based on extended state observer. *Syst. Eng. Electron.* **2019**, *41*, 1087–1093.
19. Zhang, X.J.; Liu, M.Y.; Li, Y. Backstepping sliding mode control and extended state observer based guidance law design with impact angles. *Syst. Eng. Electron.* **2017**, *39*, 1311–1316.
20. Qin, X.; Li, J.; Shao, L.; Dong, J.P.; Zhang, J.P. Guidance law with terminal attack angle constraint based on extended state observer. *J. Ballist.* **2016**, *28*, 53–58.
21. Chen, F.; He, G.J. Finite-time convergent guidance law against multipath interference. *Acta Armamentarii* **2018**, *39*, 1741–1748.
22. Zang, L.Y.; Lin, D.F.; Ji, Y. Nonsingular continuous finite-time convergent guidance law with impact angle constraints. *Int. J. Aerosp. Eng.* **2019**, *2019*, 6024240. [CrossRef]
23. Zhang, N.; Gai, W.D.; Zhong, M.Y.; Zhang, J. A fast finite-time convergent guidance law with nonlinear disturbance observer for unmanned aerial vehicles collision avoidance. *Aerosp. Sci. Technol.* **2019**, *86*, 204–214. [CrossRef]